Climate Dynamics (2006) 27: 531–541
DOI 10.1007/s00382-006-0150-8

Xavier Fettweis · Hubert Gallée · Filip Lefebre
Jean-Pascal van Ypersele

The 1988–2003 Greenland ice sheet melt extent using passive microwave satellite data and a regional climate model

Received: 2 May 2005 / Accepted: 31 March 2006 / Published online: 13 May 2006

Abstract Measurements from ETH-Camp and JAR1 AWS (West Greenland) as well as coupled atmosphere-snow regional climate simulations have highlighted flaws in the cross-polarized gradient ratio (XPGR) technique used to identify melt from passive microwave satellite data. It was found that dense clouds (causing notably rainfall) on the ice sheet severely perturb the XPGR melt signal. Therefore, the original XPGR melt detection algorithm has been adapted to better incorporate atmospheric variability over the ice sheet and an updated melt trend for the 1988–2003 period has been calculated. Compared to the original algorithm, the melt zone area increase is eight times higher (from 0.2 to 1.7% year^{-1}). The increase is higher with the improved XPGR technique because rainfall also increased during this period. It is correlated to higher atmospheric temperatures. Finally, the model shows that the total ice sheet runoff is directly proportional to the melt extent surface detected by satellites. These results are important for the understanding of the effect of Greenland melting on the stability of the thermohaline circulation.

X. Fettweis (✉) · J.-P. van Ypersele
Institut d'Astronomie et de Géophysique de G. Lemaître,
Université Catholique de Louvain, 2, chemin du cyclotron,
1348 Louvain-La-Neuve, Belgium
E-mail: fettweis@astr.ucl.ac.be
Tel.: +32-10-473302
Fax: +32-10-474722

H. Gallée
Laboratoire de Glaciologie et Géophysique de l'Environnement,
CNRS, Grenoble, France

F. Lefebre
Vito-IMS (Flemish Institute for Technological Research-Integral Environmental Studies), Mol, Belgium

1 Introduction

Understanding and estimating how the surface melting regimes of the Greenland ice sheet respond to climate variability and change becomes increasingly important, to accurately evaluate the impact of modified meltwater fluxes on the thermohaline circulation. Remote sensing has an enormous potential to monitor melt on the Greenland ice sheet. Microwave data is particularly suited because it is not obstructed by clouds. Abdalati and Steffen (1997, 2001) developed the cross-polarized gradient ratio (XPGR) method to study inter-annual melt extent variations.

We present here an inter-comparison between the Greenland melt extent simulated by a regional climate model and the one derived from satellite data with the XPGR method. The model used is the modèle atmosphérique régional (MAR) regional climate model (RCM) which will be briefly described in Sect. 2. The MAR has been extensively validated over Greenland in 1990–1991 with in-situ measurements (Lefebre et al. 2003, 2005) and satellite derived data (Fettweis et al. 2005). The passive microwave satellite data come from the Special Sensor Microwave/Imager (SSM/I) which has been operational since July 1987. They are available at a resolution of 25 km, equal to the MAR's resolution. Section 3 presents the XPGR technique from Abdalati and Steffen (1997) used to retrieve the melt. The comparison with the melt extent simulated by MAR highlights inadequacies in XPGR during rainfall events on the ice sheet (due to the presence of dense clouds). Improvements to the XPGR algorithm are presented in Sect. 4. A high correlation was found between MAR simulated runoff and satellite derived melt extent. In Sect. 5, this allows us to deduce the total ice sheet runoff from the melt extent detected by satellite. Finally, updated trends of a melt extent increase are shown in Sect. 6.

2 MAR description

The model used here is the RCM MAR coupled to the soil ice snow vegetation atmosphere transfer (SISVAT) scheme. The atmospheric part of MAR is fully described in Gallée and Schayes (1994), while the SISVAT scheme is detailed in De Ridder and Gallée (1998) and in Gallée et al. (2001). The simulation starts in September 1989 and lasts till September 2002 with a resolution of 25 km. We have used the ECMWF ERA-40 reanalysis to initialize the meteorological fields on 1 September 1989 and to force the MAR lateral boundaries every 6 h. The schemes and the setup used here are fully described in Fettweis et al. (2005) that used the first 2 years of this simulation.

3 Passive microwave satellite data

3.1 Data

The brightness temperatures used for the remote sensing melt monitoring come, respectively, from the SSM/I F-8 satellite (1987–1991), the SSM/I F-11 satellite (1992–1994) and the SSM/I F-13 satellite (1995–2003). These data are provided by the National Snow and Ice Data Center (NSIDC, Boulder, Colorado). They are arranged on a regular grid of 25 km × 25 km and are available twice a day (Armstrong et al. 1994). Before interpolating these data to the model grid, we have averaged both of the satellite passages per day as Abdalati and Steffen (1997, 2001) (noted, respectively, AS1997 and AS2001). Missing data have been corrected through linear interpolation in time if the gaps were shorter than 3 days as in Torinesi et al. (2003).

3.2 XPGR method

The approach of AS1997 is used here to deduce the melt extent over the ice sheet from the satellite data. This technique has been developed for the Greenland ice sheet by comparison with in-situ observations in the snow pack and uses multiple frequencies and polarizations to take advantage of their differing responses to the liquid water content (LWC) increase inside the snow pack. When this method detects melt, it gives the LWC of the snow pack which is very useful to compare with a model. Another algorithm has recently been developed by Torinesi et al. (2003) using only the 19-Ghz horizontal polarized brightness temperature. But (1) this technique has been calibrated/validated only in Antarctica, (2) it detects mainly the surface melt and not the massive melt as observed in Greenland and (3) it does not give the LWC equivalent of the snow pack. For these reasons, we use the AS1997 retrieval melt algorithm.

The AS1997 method is based on the XPGR, which is defined as the normalized difference between the 19-GHz horizontal polarized brightness temperature (T19H) and the 37-GHz vertical polarized brightness temperature (T37V):

$$\mathrm{XPGR} = \frac{T_b(19H) - T_b(37V)}{T_b(19H) + T_b(37V)} \quad (1)$$

A XPGR threshold value is then used to distinguish melt from non-melt points. The threshold values were determined by comparing XPGR to LWC of the snow pack at ETH-Camp (Greenland) and by intercalibration between the different data sets. The XPGR threshold was determined by AS2001 to be −0.0158 for both SSM/I F-8 and F-11 satellites and −0.0154 for the SSM/I F-13 data. The SSM/I F-11 brightness temperatures need to be intercalibrated to the F-8 baseline before using these thresholds (AS2001). When XPGR detects melt, it corresponds approximately to a LWC of 1% by volume in the top metre of snow (AS1997). We use this last criterion to distinguish melt in the MAR simulation. According to AS1997, bare ice (i.e. when the winter snow pack has completely melted and the ice appears) in the ablation zone is assumed to be melting in the model.

4 Modelled and satellite observed melt extent

4.1 Improving the original XPGR method

Fettweis et al. (2005) found that the MAR simulated extent and time evolution of the wet snow zone compare very well with the XPGR derived estimates during the 1990 and 1991 melt seasons. During rainfall events on the ice sheet, the satellite retrieved melt was however, found to be underestimated by XPGR. The 19-GHz channel is known be not very sensitive to the atmospheric variability (AS1997) but, the wavelengh of the 37-GHz channel is of the order of the diameter of water droplets in the clouds which contaminates the signal emitted by the surface.

This bias can be seen in 1991 at ETH-Camp, located some 40 km away from the ice-sheet margin, close to the long-term equilibrium line, at 1,154 m a.s.l. XPGR detects melt when the LWC is above 1% by volume in the top metre of snow. Figure 1 plots here the LWC of the observed snow pack above the ice (Ohmura et al. 1992). The LWC reaches values above 1% during the whole period shown in Fig. 1, except in mid-June although XPGR detects melt. During this period, the height of the observed snow pack is about 1.4 m and the LWC of the top metre of snow is higher than the LWC of the total snow pack because the melt water has not yet reached the depths of the snow pack at the beginning of the melt season. That is why XPGR detects melt during this event. At the end of August, although the 2 m-temperature is below 0°, the snow pack is still detected as melting by XPGR because the freezing surface temperatures are not low enough to refreeze the liquid melt water from deeper area. However, XPGR fails several

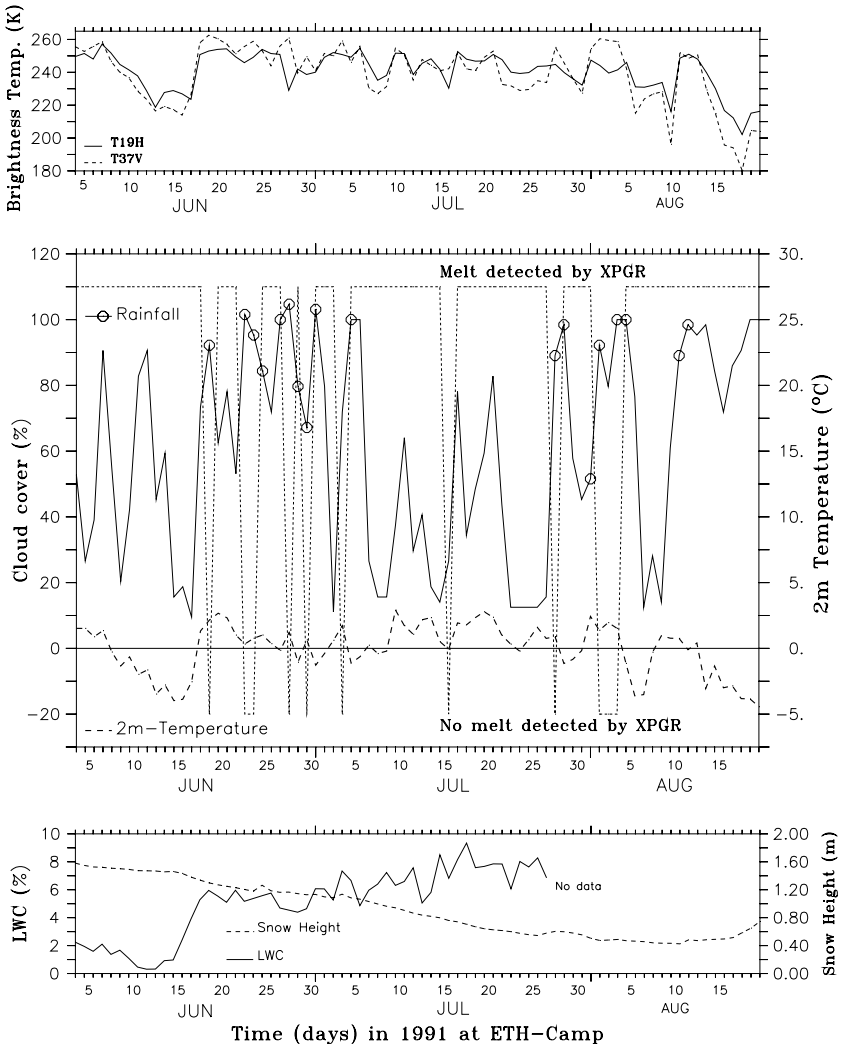

Fig. 1 *Top* the 19-GHz horizontal polarized brightness temperature (*solid*) and the 37-GHz vertical polarized brightness temperature (*dashed*) from SSM/I F-8 satellite at ETH-Camp. *Middle* the daily means of the cloud cover (*somlid*) observed at ETH-Camp. The *circles* on the curve indicate the days when rainfall was observed at ETH-Camp in 1991 (Ohmura et al. 1992). Also shown is the observed 2 m-temperature (*dashed*) at ETH-Camp in 1991 (Ohmura et al. 1992). Finally, the *dotted curve* shows when XPGR (AS1997) detects melt: above zero when XPGR detects melt, below zero otherwise. *Below*: the snow height (*dashed*) and its LWC (*solid*) observed at ETH-Camp. The ImpXPGR algorithm detects melt during the whole period (not shown). In detail: improvement no. 1 accounts for 11 days, improvement no. 2 for 0 days, improvement no. 3 for 0 days and improvement no. 4 for 0 days

times to detect melt because the T37V is too warm, while the LWC of the snow pack is above 1% and the 2 m-temperature is above the freezing point. Rainfall was observed at ETH-Camp in most of these cases which suggests perturbations in the remote observed melt signal.

Some abnormal short gaps in the melt season detected by XPGR can also be seen in Fig. 2 at the JAR1 automatic weather station (AWS) from the Greenland Climate Network (GC-Net). This AWS is situated underneath ETH-Camp at 962 m a.s.l. in the ablation zone. During the warm 1998 summer, the snow pack was observed to melt about 2.4 m of water equivalent, continuously from 24 May until the end of September (Steffen and Box 2001). XPGR fails several times to detect melt during some days in the melt season when (1) it detects melt some days before/after the day considered and (2) the observed (and simulated) 2 m-temperature remains positive during each of these small episodes. Therefore the snow pack should continue to be detected as melting during these days as it was observed on the site (Steffen and Box 2001). For almost each of them, low shortwave incoming radiative fluxes were measured at JAR1 indicating dense clouds, and rainfall was simulated by MAR most of the time. A rainfall/snowfall episode at the end of May postpones the melt onset to the 28 of May in XPGR fields. After 7 September the snow pack begins to refreeze from the surface due to lower air temperatures, but the snow pack is still detected as melting because of the deeper liquid melt water. The improved XPGR algorithm (see below) and MAR detect successfully melt continuously from 22 May to the end of September (not shown here). Finally, a good agreement between the measured and modelled 2m-temperature was highlighted in Fig. 2.

The perturbations, as discussed in the paragraph before, are largely due to dense clouds in the XPGR melt signal. This is also highlighted in Figs. 3 and 4 where abnormal low melt signals detected by XPGR are mostly associated to rainfall events simulated by MAR. Hence the XPGR algorithm must be improved to better incorporate the atmospheric variability. During rainfall events notably, XPGR does not detect melt most of the time because T37V is abnormally high. The ideal solution would be to correct T37V but it is difficult to detect efficiently the perturbations due to atmospheric

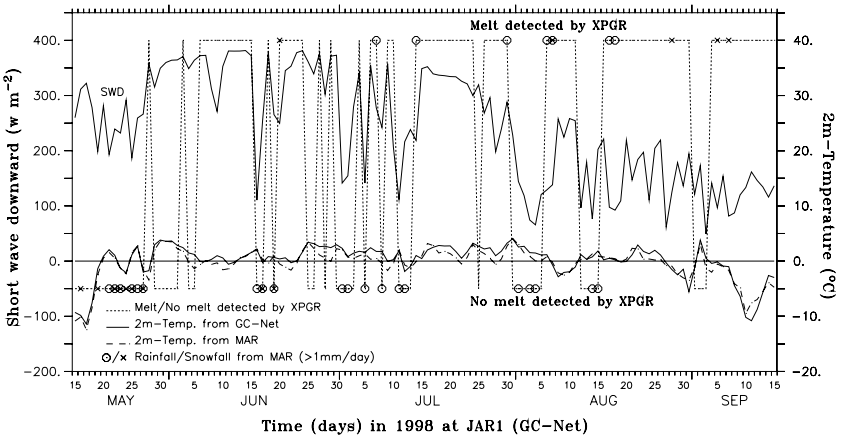

Fig. 2 The *solid lines* show the daily means of the incoming shortwave (*top*, left axis) and the 2m-temperature (*bottom*, right axis) measured at the JAR1 AWS in the summer of 1998 (Steffen and Box 2001). The *dotted curve* shows when XPGR (AS1997) detects melt: above zero when XPGR detects melt, below zero otherwise. The 2m-temperature simulated by MAR is plotted with a *dashed line*. Days on which MAR simulates rainfal (respectively, snowfall) higher than 1 mm/day are indicated by *circles* (respectively, crosses). Finally, the ImpXPGR algorithm and MAR detect melt continuously from 22 May to the end of September (not shown here). The ImpXPRG algorithm detects 42 more melt days than XPGR in 1998 at JAR1. In detail: improvement no. 1 accounts for 34 days, improvement no. 2 for 6 days, improvement no. 3 for 2 days and improvement no. 4 for 0 days

variability. Therefore, we propose four different improvements to the XPGR algorithm. The original XPGR melt retrieval algorithm from AS1997 together with these fours improvements is denoted hereafter ImpXPGR.

(1) We impose the continuity of the melt season to remove gaps shorter than 3 days between two melting days. The XPGR method is aimed to detect massive melt, i.e. when the LWC is higher than 1% in the top metre of snow. Therefore short gaps in the middle of the melt season detected by XPGR, as those shown at ETH-Camp and at JAR1 AWS, are mostly unrealistic. They are in general found to be associated with dense clouds mostly causing precipitation on the ice sheet. It is clear that the snow pack continues to melt when it is raining. When it is snowing, the fresh snow layer above the melting snow pack is normally insufficient to decrease the LWC below 1% in the top metre of snow. In the middle of the summer, a snow pack with a LWC of 2% and more is usual and therefore more than 50 cm of fresh snow is needed so that the pixel is not detected as melting any more. Rather than dry fresh snow addition, lower temperatures that refreeze the melt water deeper in the snow pack can efficiently mask the melt signal. However, as shown at ETH-Camp and at JAR1 AWS, periods of refreeze during the melt season lasting less than 3 days are too short to refreeze in depth the liquid melt water which prolongs the remote detection of the melt (AS1997). XPGR without corrections detects successfully melt during these refreeze events. The satellites stops to detect melt at the end of the ablation season until the subsurface snow has refrozen. This correction constitutes the main improvement as shown both in Figs. 4g and 5.

(2) Pixels situated at lower altitudes than three adjacent pixels where XPGR detects melt are classified as melting pixels. Indeed, the true resolution of T19H is 69×43 and 37×28 km^2 for T37V. These values are then interpolated on a regular grid (25 km $\times$ 25 km) by the NSIDC. Therefore, the signal emitted by the ice sheet margin pixels near sea, fjord or fresh melt water lake, in the tundra or on the ice sheet are contaminated by the water signal which is very different from the snow/ice signal. This second correction allows to resolve this problem to a large extent. Nevertheless, the intersection of both MAR and AS1997 ice sheet mask (removing a part of MAR ice sheet margin pixels) is used in both Figs. 3 and 4 for a better comparison between XPGR and the improved XPGR.

(3) For each year, we compute the mean T19H temperature and the standard deviation over time and over all the grids points where XPGR [+ corrections (1) and (2)] detects melt. We add half of the mean standard deviation to this average. This computed value is spatially constant and varies only interannually around 235 K to take into account differences between the three satellites of SSM/I data as the XPGR threshold. If T19H is above this value, we assume that melt takes place. On the one hand, to remove eventual anomalies in SSM/I brightness temperature fields. On the other hand, to detect melt along the ice sheet margin. It is a correction à la Torinesi et al. (2003). The 19-GHz channel is chosen because it is the least sensitive to the atmospheric variability. As for the second improvement, this correction improves the remote melt detection along the ice sheet margin (see Fig. 5).

(4) As for the third improvement, we compute the mean T19H temperature and the standard deviation

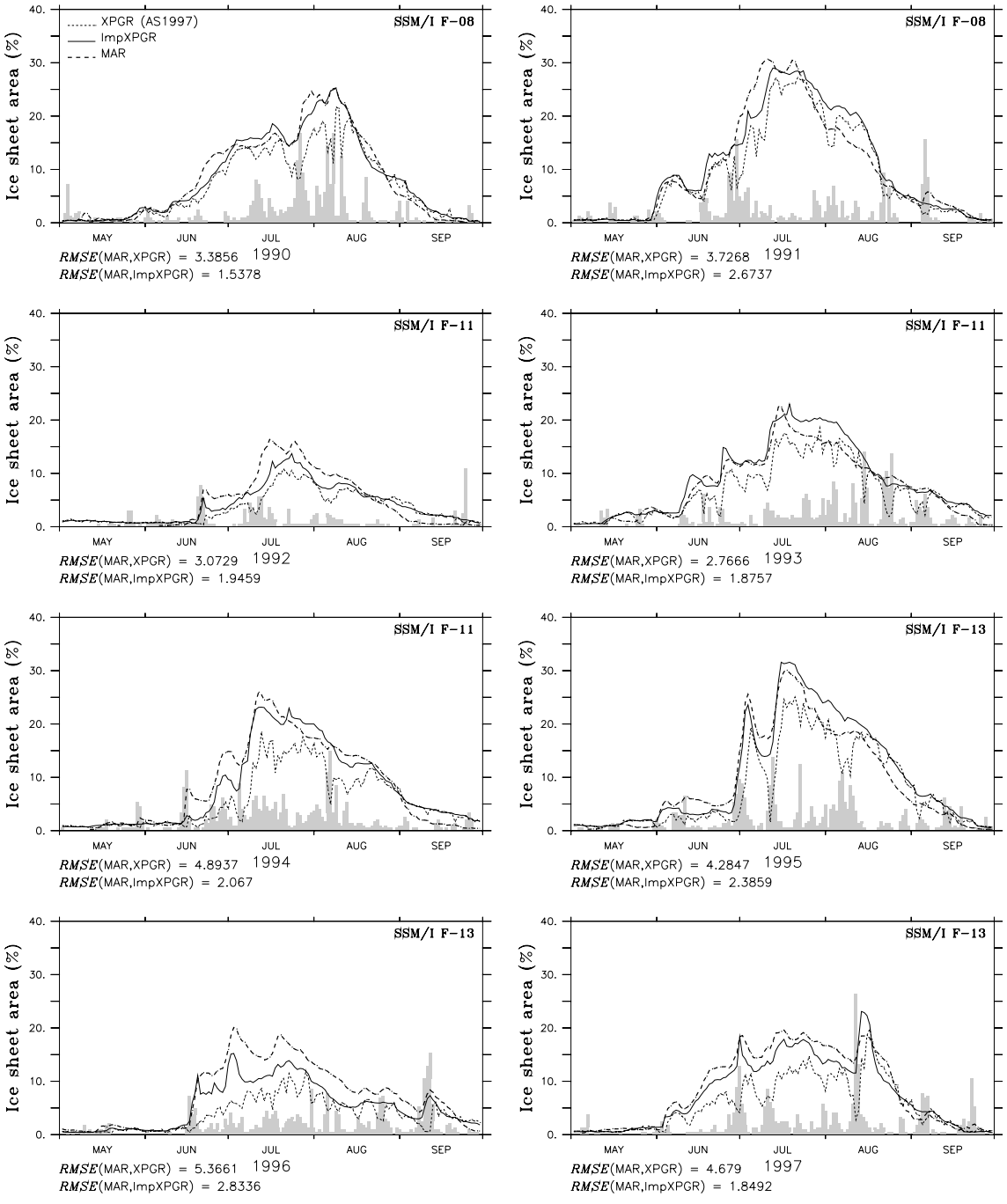

Fig. 3 Daily mean melt zone extent detected by XPGR from AS1997 (*dotted*), by the improved XPGR (ImpXPGR) (*solid*) and simulated by MAR (*dashed*) for 1990–1997. Melt is expressed in percentage of the Greenland ice sheet area that lies in the intersection of both MAR and AS1997 ice mask (which covers 1.56×10^6 km^2). Also shown is the percentage of Greenland ice sheet area where MAR simulates daily rainfall greater than 1 mm/day (*grey bars*)

but now when XPGR does not detect melt. We subtract half of the mean standard deviation from this average. To remove anomalies in remote sensing observation, "no melt" is imposed if T19H is lower than this value (around 176 K). The third improvement adds melting pixels to the melt detected by the original XPGR at the beginning of the ablation season whereas the fourth improvement removes rather melting pixels at the end of the ablation season (See Fig. 4g).

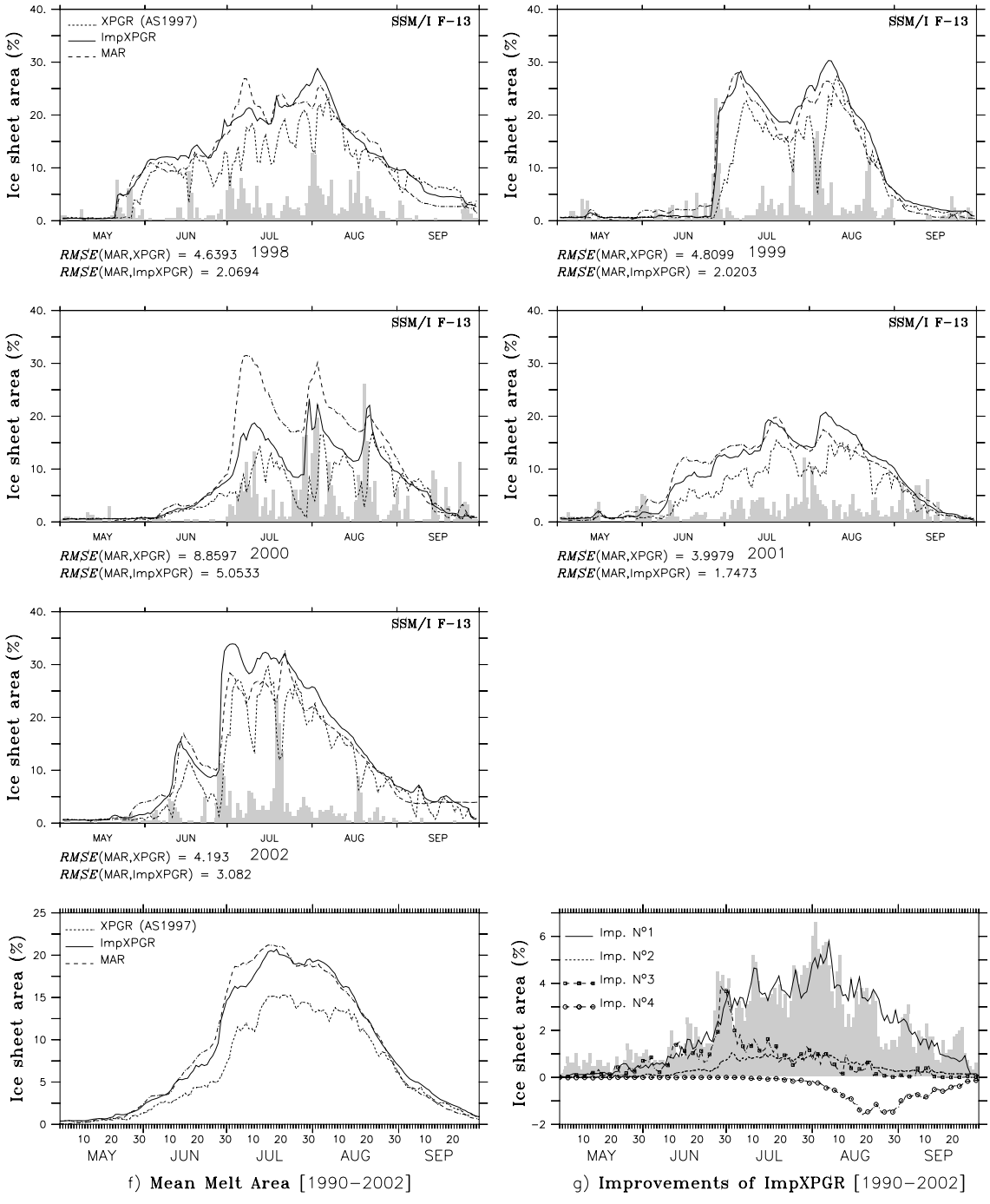

Fig. 4 Same as Fig. 3 but for 1998–2002. The last two plots (**f, g**) show the mean melt area for 1990–2002 and the mean relative effects of the four improvements of ImpXPGR to the original XPGR algorithm (AS1997) presented in sect. 4.1. Also shown in **g** is the 1990–2002 mean percentage of Greenland ice sheet area in which MAR simulates daily rainfall greater than 1 mm/day (*grey bars*). Note that the vertical axis scales of the last two plots are different than before

4.2 Comparison

The agreement between the MAR simulated and the satellite retrieved melt becomes significantly better (Figs. 3, 4, 6) when ImpXPGR is used. The statistics are summarised in Table 1. MAR compares better with XPGR when rainfall/snowfall pixels are removed according to Fettweis et al. (2005). The removal of rainfall pixels does not improve the comparison with ImpXPGR because this last corrects the melt detection during rainfall. When snowfall pixels are removed, the agreement with ImpXPGR is better but the number of pixels taken into account in the comparison is significantly reduced. The yearly RMSE are shown in Figs. 3 and 4 below each plot. The abnormally low satellite derived melt signal due to rainfall events are now

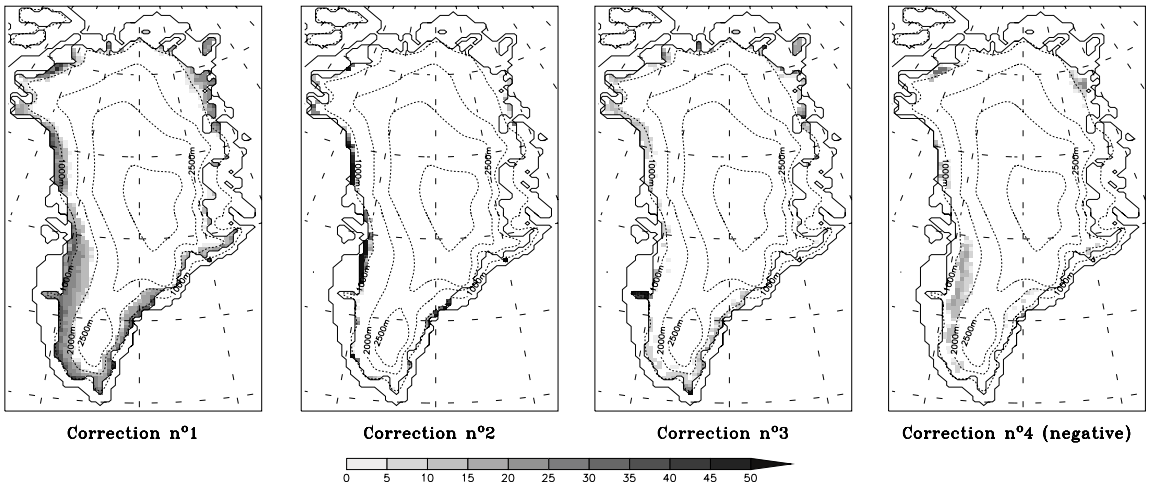

Fig. 5 The number of ablation days per year, averaged over the 1990–2002 period, changed by the four corrections of ImpXPGR in comparison to the original XPGR algorithm detection. The first three improvements of ImpXPGR add melting days to original XPGR algorithm detection. The last one from which the absolute value is shown here removes melting days. The relative effect of each improvement is also indicated in *brackets*. Finally, this figure explains the differences between Figs. 6a, b

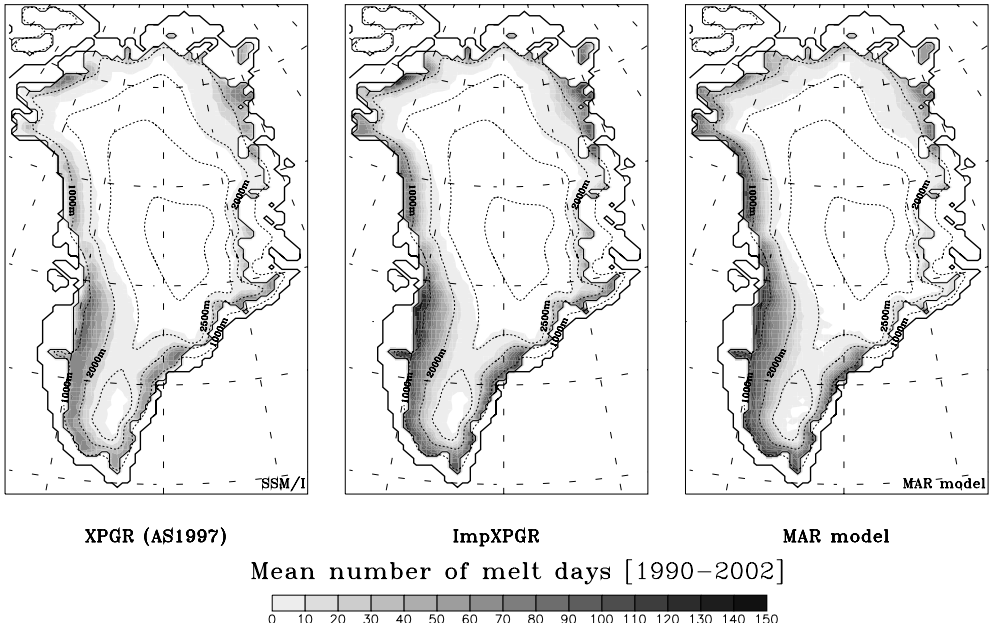

Fig. 6 Yearly mean total number of ablation days detected by XPGR from AS1997 (*left*), by ImpXPGR (*middle*) and simulated by MAR (*right*)

corrected in a large part. See, for example, in Figs. 3 and 4 the improvements during the following time periods: 22–27 July 1990, 27–30 June 1991, 23–24 August 1993, 11–12 July 1995, 9–11 September 1996, 3 August 1999, 28–29 July 2000, and multiple episodes during the melt record years 1998 and 2002. The maximum melt extent area in July 2002 (Steffen et al. 2004) is well simulated. The minimum occurs in summer 1992 due to the eruption of Mount Pinatubo (AS2001). The rainfall perturbations in the XPGR signal become insignificant at the end of melt season when the melt signal is then emitted only by sub-surface melt water (see both last plots of Fig. 4). When the surface begins to refreeze, the melt signal comes mainly from the T19H channel which is less sensitive to the cloud liquid water contrary to the T37V channel.

Both MAR and ImpXPGR detect much more melt than XPGR along the ice sheet margins (Fig. 6). Indeed, the closer a pixel is to the ice sheet margin, the higher the probability to have rainfall or clouds with liquid water and the higher the probability that XPGR is biased. As already pointed out by Fettweis et al. (2005), MAR simulates less melt along the eastern and south-eastern mountainous regions of the ice sheet than the XPGR and the ImpXPGR estimates (Fig. 6). MAR likely overestimates (solid) precipitation in this region which reduces melt (Fettweis et al. 2005), but microwave brightness temperatures could be biased by numerous

Table 1 The 1990–2002 mean melt extent, correlation coefficient and root mean-square error (RMSE) between melt extent simulated by MAR and derived from SSM/I remote sensing observations by XPGR and ImpXPGR algorithms

	MAR	XPGR	ImpXPGR
Mean melt extent	8.73%	6.33%	8.62%
Mean melt extent (without rainfall pixels)	7.66%	6.08%	7.72%
Mean melt extent (without snowfall pixels)	6.01%	4.79%	6.3%
Correlation coefficient with MAR		0.87	0.95
Correlation coefficient with MAR (without rainfall pixels)		0.90	0.95
Correlation coefficient with MAR (without snowfall pixels)		0.90	0.95
RMSE with MAR		4.76%	2.56%
RMSE with MAR (without rainfall pixels)		3.64%	2.44%
RMSE with MAR (without snowfall pixels)		3.04%	2.10%

According to Fettweis et al. (2005), MAR versus XPGR "without rainfall/snowfall pixels" means that all the grid points with MAR daily liquid/solid precipitation greater than 1 mm/day have been not considered in the computation. The RMSEs and averages are expressed in percentage of the Greenland ice sheet area that lies in the intersection of both MAR and AS1997 ice mask (which covers 1.56×10^6 km^2)

rock outcrops (boulders) found in this mountainous region (Torinesi et al. 2003).

5 Runoff

Mote (2003) uses a positive degree day (PDD) model to deduce the runoff of the Greenland ice sheet from the satellite derived melt extent. Here we propose an estimation of the total ice sheet runoff coming from the melt extent surface detected by ImpXPGR. It is clear that ImpXPGR cannot be used directly to quantify locally the runoff because it is based on a threshold value. Moreover, the runoff comes mainly from the low altitude regions along the ice sheet margin while ImpXPGR sometimes detects melt up to the crest of the ice sheet. However the more extended the melt area, the higher the melt takes place, the stronger the melt will be and will be the runoff. This hypothesis is confirmed in Fig. 7 where a high correlation of 0.93 (respectively, 0.84) is found between the 1990–2002 daily total ice sheet runoff simulated by MAR and the ImpXPGR (respectively, XPGR) melt area. Based on this hypothesis and on the MAR results, an empirical estimation of the Greenland ice sheet runoff is made from the ImpXPGR melt extent via this linear regression:

$$\mathrm{Ru}_{\mathrm{SSM/I}} = \mathrm{ME}_{\mathrm{SSM/I}} \times 80.4810^{-7} - 0.19 \qquad (2)$$

where $\mathrm{Ru}_{\mathrm{SSM/I}}$ is the total ice sheet runoff in km^3 year^{-1} and $\mathrm{ME}_{\mathrm{SSM/I}}$ is the melt extent in km^2 year^{-1} detected by ImpXPGR. The coefficients of the regression line are of course "model dependent". But, as far as we assume the linearity in this estimation to be correct, an increase of the melt extent (easily detected by satellite) corresponds to an increase of the ice sheet runoff in the same proportions, no matter the runoff value. The 1990–2002 RMSE between the MAR runoff and the ImpXPGR (respectively, XPGR) derived runoff estimation is 0.53 (respectively, 0.75) km^3. By comparison with Mote (2003) and Box et al. (2004) estimations, the runoff simulated by MAR (and then derived from SSM/I) is lower (see Fig. 8), but it must be noted that the agreement with the satellite melt data is good.

The linear relation has a negative intercept. ImpXPGR detects melt when the LWC of the top metre of snow is higher than 1%. Before running off, a part of the meltwater is retained inside the snow pack assuming a maximum value for the LWC or can accumulate above ice or snow layers having high densities or being saturated by liquid water. The runoff of excessive internal and accumulated surface meltwater in MAR model is based on the work of Zuo and Oerlemans (1996) and described more in detail in Lefebre et al. (2003). The maximum value of the LWC is chosen to be 0.07 according to Colbeck (1974) and corresponds approximatively to a LWC of 3.5% by volume in the top metre of snow that has a density of 500 kg/m^3 which is a typical value for a melting snow pack. Therefore,

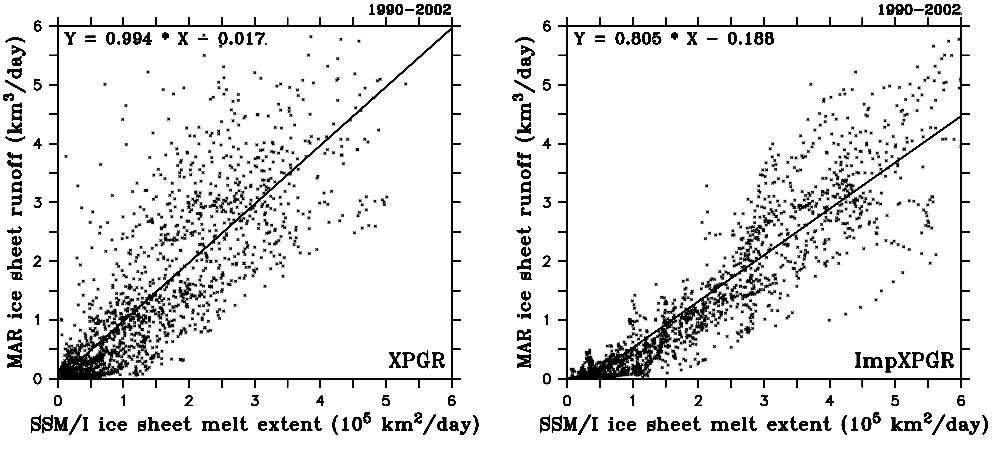

Fig. 7 Comparison between the total ice sheet runoff simulated by MAR (in mm) and the melt extent detected by XPGR (*left*) and ImpXPGR (*right*) (in 10^5 km^2) for the period 1990–2002. The regression line is also plotted

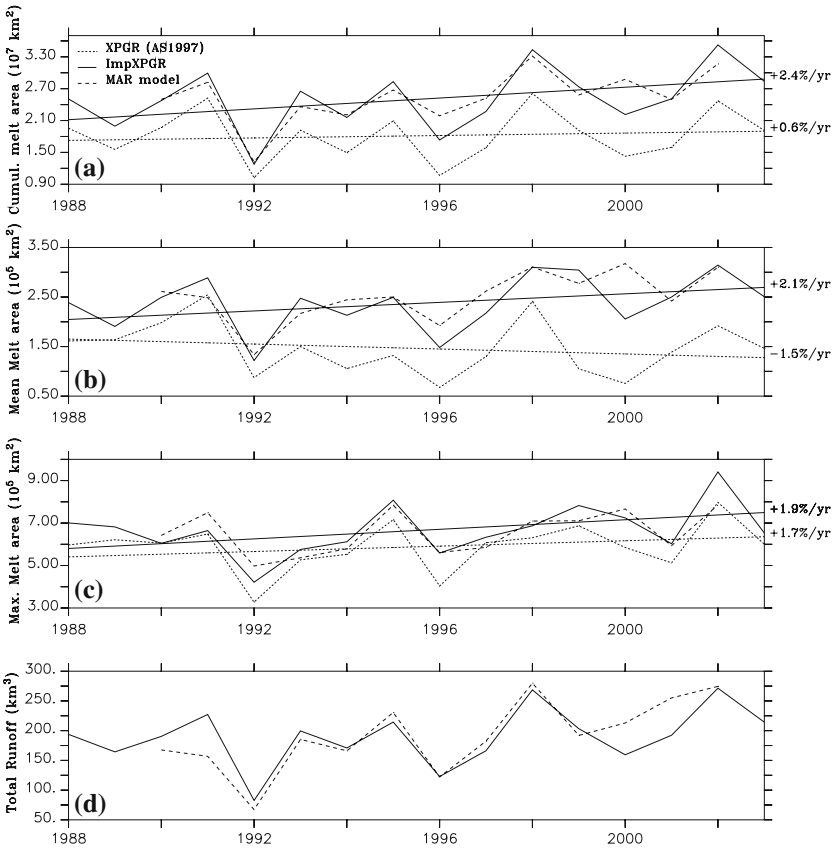

Fig. 8 **a** Annually cumulated melt area detected by XPGR from AS1997 (*dotted*), by ImpXPGR (*solid*) and simulated by MAR (*dashed*). **b** Annually averaged summer mean melt extent defined by AS1997 (June–August). **c** Maximum melt extent of the ice sheet as in Steffen (2002). **d** Total ice sheet runoff simulated by MAR and derived from the melt extent detected by ImpXPGR. The trends for XPGR (*dotted*) and ImpXPGR (*solid*) are also shown

ImpXPGR detects the meltwater at the beginning of the ablation season before it can be run off in MAR, which explains the negative constant in the regression.

6 Melt trend estimates

Between 1988 and 2003, XPGR and ImpXPGR, respectively detect over the Greenland ice sheet an average increase of the cumulated melt extent of 0.2% year^{-1} ($+0.003 \times 10^7$ km^2 year^{-1}) and of 1.7% year^{-1} ($+0.038 \times 10^7$ km^2 year^{-1}) (Fig. 8a). The cumulated melt extent is defined as the annual total sum of every daily ice sheet melt area. This trend corresponds to a melt area increase of respectively, $+0.049 \times 10^7$ and $+0.581 \times 10^7$ km^2 from 1988 to 2003 with a significance of about 85% for ImpXPGR. The significance has been tested using a Monte-Carlo method with 1,000,000 simulations of autocorrelated data series with the same autocorrelation as the ImpXPGR time series. According to the previous section, we find this same trend in the total runoff of the ice sheet. The positive trend is higher with ImpXPGR because, as showing the ERA-40 reanalysis and MAR, rainfall on the ice sheet increases with temperature (Box 2002). For the summers 1990–2002, MAR simulates an 0.20°C year^{-1} increase of the mean air temperature above the ice sheet and an increase of the total rainfall on the ice sheet of 1.2 mm year^{-1}. The trends of the mean melting area in June–August as defined by AS1997 (Fig. 8b) and of the maximum melting area as Steffen (2002) (Fig. 8c) are also shown. But the cumulated melt area parameter is a better indicator of the total melt of the year.

The melt zone extension lies mainly in the northern part of Greenland (especially the Humboldt Glacier) and along the western coast in the higher ablation zone and in the percolation zone (Fig. 9). In the lower western ablation zone, no change is detected by the satellites because melt occurs already almost always during the melt season (see Fig. 6). Except near Tunu in the percolation zone, the changes are very low along the eastern coast and the trend is even negative on the Greike Plateau. In this region, the trends (1990–2002) simulated by MAR are an increase of the snowfall, a decrease of rainfall and no temperature change which can explain the observed melt trends. Indeed, more snowfall and less rainfall decrease the LWC in the snow pack, raise the albedo and therefore reduce the melt. Finally, these regional trends are in agreement with AS2001 (see their Fig. 3).

7 Conclusion

A comparison between the Greenland melt extent simulated by the regional climate model MAR and derived from SSM/I satellite data has been performed. This has highlighted some biases during rainfall events in the XPGR algorithm (AS1997) used to retrieve melt area

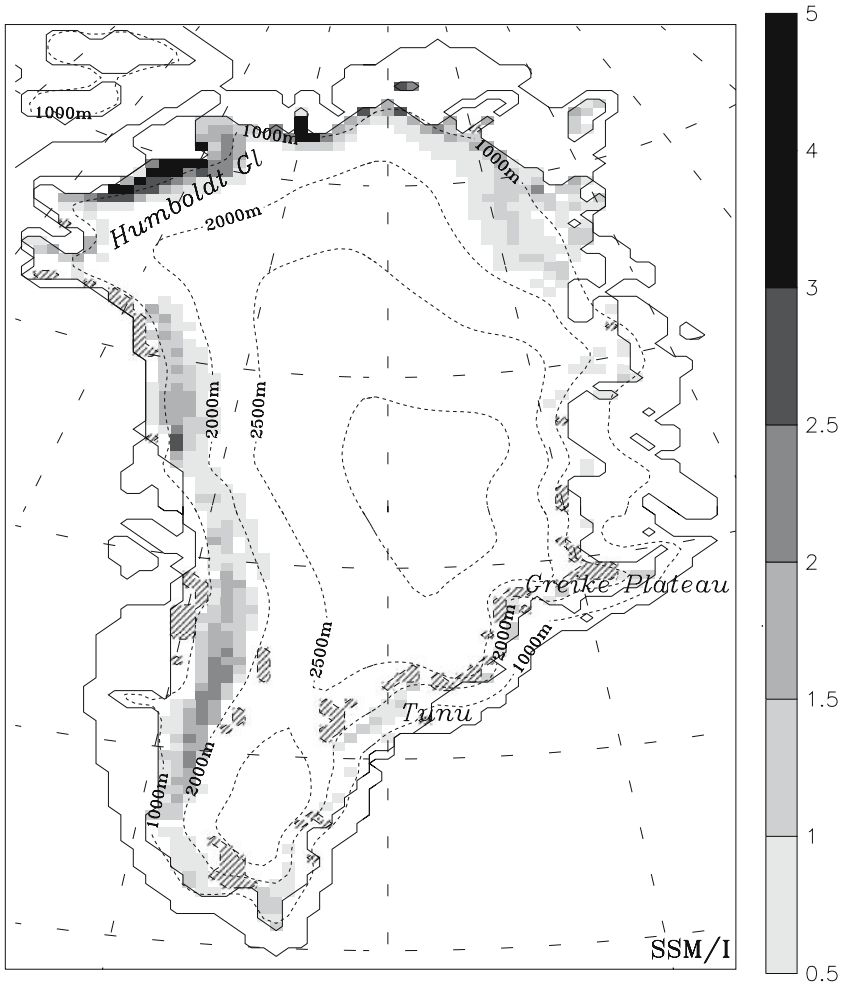

Fig. 9 Melt trend in (ablation days) $(\text{year})^{-1}$ detected by ImpXPGR for the period 1988–2003. Negative trends are hatched. This map shows also the locations (*italic*) quoted in the text

from passive microwave satellite data. The XPGR technique has been improved to correct the abnormally low satellite derived melt signals during rainfall events. The agreement with the model has became clearly better. The improved XPGR method shows a cumulated melt area increase of 1.7% year^{-1} ($+0.038 \times 10^7$ km^2 year^{-1}) for the period 1988–2003 (with a significance of about 85%). This increase is mainly situated in the North and along the West coast of Greenland in the ice sheet percolation zone. In the lower western ablation zone, no change is detected by the satellites because melt occurs already almost always during the melt season. The non-modified XPGR technique shows a lower change because the rainfall on the ice sheet has also increased which partly masks the melt increase.

Since 1988, the cumulated melt extent on Greenland has increased by almost 30%. This trend agrees with recent observations highlighting rapid and substantial changes on the Greenland ice sheet due to a climate warming (Krabill et al. 2000; Rignot and Thomas 2002; Schiermeier 2004). Moreover, the melt of the Greenland ice cap may be irreversible (Toniazzo et al. 2004). By using model results, we have shown that the total Greenland ice sheet runoff is directly proportional to the melt extent detected by the satellite. Therefore it is probable that the runoff has also increased in the same proportions which combined to an ice discharge increase (Zwally et al. 2002) gives an increasing fresh water flux to the North-Atlantic ocean. These results are important for the understanding of the effect of Greenland melting on the stability of the thermohaline circulation.

Acknowledgments Xavier Fettweis is a research fellow of the Belgian National Fund for Scientific Research. The authors acknowledge the National Snow and Ice Data Center (NSIDC, Boulder, Colorado) for providing the passive microwave satellite data from SSM/I (see http://www.nsidc.org/). The authors acknowledge also Dr. Konrad Steffen for providing the GC-Net AWS measurements of 1998. The project was supported by the French programme ACI-C3 (Ministère de la Recherche). All major computations were realized with IDRIS computing resources (France).

References

Abdalati W, Steffen K (1997) Snowmelt on the Greenland ice sheet as derived from passive microwave satellite data. J Clim 10:165–175

Abdalati W, Steffen K (2001) Greenland ice sheet melt extent: 1979–1999. J Geophys Res 106:33983–33989

Armstrong RL, Knowles KW, Brodzik MJ, Hardman MA (1994) DMSP SSM/I Pathfinder daily EASE-Grid brightness temperatures, May–September 1990 & 1991. Boulder, CO: National Snow and Ice Data Center. Digital media and CD-ROM

Box JE (2002) Survey of Greenland instrumental temperature records: 1873–2001. Int J Climato 22:1829–1847

Box JE, Bromwich DH, Bai L-S (2004) Greenland ice sheet surface mass balance for 1991–2000: application of Polar MM5 mesoscale model and in-situ data. J Geophys Res, vol. 109, No. D16, D16105, 10.1029/2003JD004451

Colbeck SC (1974) The capillary effects on water percolation in homogeneous snow. J Glaciol 13(67):85–97

De Ridder K, Gallée H (1998) Land surface-induced regional climate change in Southern Israel. J Appl Meteorol 37:1470–1485

Gallée H, Schayes G (1994) Development of a three-dimensional meso-γ primitive equations model. Mon Wea Rev 122:671–685

Gallée H, Guyomarc'h G, Brun E (2001) Impact of the snow drift on the Antartic ice sheet surface mass balance: possible sensitivity to snow-surface properties. Boundary-Layer Meteorol 99:1–19

Fettweis X, Gallée H, Lefebre L, van Ypersele J-P (2005) Greenland surface mass balance simulated by a regional climate model and comparison with satellite derived data in 1990–1991. Climate Dynamics, No. 24:623–640, DOI: 10.1007/s00382-005-0010-y

Krabill W, Abdalati W, Frederick E, Manizade S, Martin C, Sonntag J, Swift R, Thomas R, Wright W, Yungel J (2000) Greenland ice sheet: high-elevation balance and peripheral thinning. Science 289:428–430

Lefebre F, Gallée H, van Ypersele J, Greuell W (2003) Modeling of snow and ice melt at ETH-camp (west Greenland): a study of surface albedo. J Geophys Res 108 No. D8, 10.1029/2001JD001160

Lefebre F, Fettweis X, Gallée H, van Ypersele J, Marbaix P, Greuell W, Calanca P (2005) Evaluation of a high-resolution regional climate simulation over Greenland. Climate Dyn, DOI: 10.1007/s00382-005-0005-8

Mote TL (2003) Estimation of runoff rates, mass balance, and elevation changes on the Greenland ice sheet from passive microwave observations. J Geophys Res 108(D2):4056, DOI:10.1029/2001JD002032

Ohmura A, Steffen K, Blatter H, Greuell W, Rotach M, Stober M, Konzelmann T, Forrer J, Abe-Ouchi A, Steiger D, Niederbaumer G (1992) Energy and mass balance during the melt season at the equilibrium line altitude, Paakitsoq, Greenland ice sheet: Progress report 2, Department of Geography, Swiss Federal Institute of Technology, Zurich

Rignot E, Thomas R (2002) Mass balance of polar ice sheets. Science 297:1502–1506

Schiermeier Q (2004) Greenland's climate: a rising tide. Nature 428:114–115, DOI:10.1038/428114a

Steffen K (2002) Greenland maximum melt extent available on http://www.cires.colorado.edu/steffen/melt/

Steffen K, Box JE (2001), Surface climatology of the Greenland ice sheet: Greenland climate network 1995–1999. J Geophys Res 106(D24):33,951–33,964

Steffen K, Nghiem SV, Huff R, Neumann G (2004) The melt anomaly of 2002 on the Greenland Ice Sheet from active and passive microwave satellite observations. Geophys Res Lett 31:L20402, DOI:10.1029/2004GL020444

Toniazzo T, Gregory JM, Huybrechts P (2004) Climatic impact of a Greenland deglaciation and its possible irreversibility. J Clim 17:21–33

Torinesi O, Fily M, Genthon C (2003) Variability and trends of the summer melt period of Antarctic ice margin since 1980 from microwave sensors. J Clim 16:1047–1060

Zuo Z, Oerlemans J (1996) Modelling albedo and specific balance of the Greenland ice sheet: calculations for the Sondre Stromfjord transect. J Glaciol 42(141):305–317

Zwally JH, Abdalati W, Herring T, Larson K, Saba J, Steffen K (2002) Surface melt-induced acceleration of Greenland ice-sheet flow. Science 297:218–222